Journal of Membrane Science 635 (2021) 119428

Contents lists available at ScienceDirect

Journal of Membrane Science

journal homepage: www.elsevier.com/locate/memsci

Printing zwitterionic self-assembled thin film composite membranes: Tuning thickness leads to remarkable permeability for nanofiltration

Xin Qian [a], Tulasi Ravindran [a], Samuel J. Lounder [b], Ayse Asatekin [b], Jeffrey R. McCutcheon [a,*]

[a] Department of Chemical & Biomolecular Engineering, Center for Environmental Sciences and Engineering, University of Connecticut, Storrs, CT, USA
[b] Department of Chemical & Biological Engineering, Tufts University, Medford, MA, USA

ARTICLE INFO

Keywords:
3D printing
Self-assembly
Nanofiltration
Zwitterion
Copolymer
Additive manufacturing

ABSTRACT

Zwitterionic copolymer self-assembled membranes have been shown to have impressive selectivity for nanofiltration applications. Conventional approaches used to fabricate these asymmetric membranes, such as casting followed by phase inversion, typically result in thick selective layers being formed that can limit permeance. In this work, we evaluate the use of electrospray to print thin layers of amphiphilic zwitterionic selective layers onto UF membrane substrates. Dyes are used to probe the rejection of these membranes while their thickness is reduced by orders of magnitude compared to casting methods. As thickness is decreased, water permeance was found to proportionally increase while dye rejection was maintained for some dyes. It was found that a threshold minimum thickness was required to maintain rejection for some dye molecules while the intrinsic permeability of the polymer films changed as a function of thickness. Annealing the membranes was found to increase permeance as well without a significant loss of rejection. Notably, one of our annealed ultra-thin TFC membranes was found to exhibit a water permeance value of 180 LMH/bar and a chlorophyllin rejection at 99.67%. Interestingly, this permeance is indistinguishable from the supporting UF membrane permeance, suggesting that even higher permeance without rejection loss is possible with more permeable support layers.

1. Introduction

Membranes are an inherently tunable platform for providing various types of separations in water treatment [1–3]. Through tuning of membrane materials as well as adapting those materials to new manufacturing approaches, membranes can offer selectivity of water over macromolecules (ultrafiltration UF), multivalent salts and small molecules (nanofiltration NF), and monovalent salts (reverse osmosis, RO). UF membranes are typically made from a process known as non-solvent induced phase precipitation (NIPS) [4] where an integrated skin layer is formed on a support layer of identical material. The development of modern NF [5] and RO [6] membranes saw the emergence of the thin film composite (TFC) membrane, which is a structure where a materially distinct selective layer is formed independent from the supporting structure. TFC membranes were first developed by Cadotte [7] who conducted interfacial polymerization *in situ* on a porous membrane substrate to form a polyamide selective layer. In recent years, many studies have either enhanced the permeance and antifouling performance of polyamide TFC membrane by integrating filler material into the selective layer [8] or expanded the application of TFC membranes in organic solvent NF [9,10], seawater desalination RO [11], pervaporation and gas separation [12].

Remarkably, thin film composite membrane structures and chemistries have changed little over the last 40 years. These membranes commonly use a polysulfone-based polymer that is cast by NIPS onto a polyester nonwoven scrim as a support for ultra-thin and mechanically fragile selective layer. These selective layers are almost exclusively polyamides and are formed via interfacial polymerization as a diamine monomer reacts with an acid chloride at the interface between an organic and aqueous phase [13]. Alternative materials have been considered, but none have had the exceptional permeance combined with selectivity and manufacturability of polyamides.

Self-assembling materials have gained recent prominence as a potential membrane material due to their ability to form pore domains of narrow size distribution. Self-assembly is a spontaneous organization of molecules or structures driven by interactions between ionic or polar groups [14]. These polymers have clearly separated hydrophobic and hydrophilic domains which provide for high water flux and fouling

* Corresponding author. Department of Chemical & Biomolecular Engineering, Center for Environmental Sciences and Engineering, University of Connecticut, Storrs, CT, USA.
E-mail address: jeffrey.mccutcheon@uconn.edu (J.R. McCutcheon).

https://doi.org/10.1016/j.memsci.2021.119428
Received 11 November 2020; Received in revised form 4 May 2021; Accepted 7 May 2021
Available online 27 May 2021

resistance. Many researchers have reported on self-assembled polymer nanostructures for liquid filtration membranes [15–24]. While these studies exemplify the potential of self-assembling materials for membrane applications, they also demonstrate the importance of simple, scalable manufacturing methods for forming thin selective layers where self-assembly can still occur.

Zwitterionic copolymers are considered an anti-fouling materials for membranes because of their chemistry and hydrophilicity [25]. Interestingly, they have also been identified as materials that self-assemble to create domains that could be used to provide molecular-scale separation. Self-assembly of zwitterionic copolymers in particular is driven by strong dipole-dipole interaction between zwitterions and the difference in hydrophilicity between the copolymer and zwitterion domains [26]. The resulting structure is an interconnected network of water channels that are both narrow in their size to provide selectivity and hydrophilic to provide permeability. TFC membranes prepared by casting the self-assembling zwitterionic amphiphilic copolymer poly(trifluoroethylmethacrylate-*random*-sulfobetaine methacrylate) (PTFEMA-*r*-SBMA) on a PVDF support are extremely fouling-resistant with sharp size based rejections for small organic molecules less than 1 nm in size [26–28]. Bengani et al. [27]also explored the impact of zwitterionic copolymer chemical structure in membrane morphology and properties such as flux and antifouling performance by comparing four different zwitterionic copolymers with varying zwitterion density and linker groups. In another paper [28], they demonstrated the superior fouling resistance and chemical tolerance of these zwitterionic copolymer membranes in treating municipal oily and textile wastewaters. These studies used TFC membranes made by coating a thin layer of copolymer onto a large pore size membrane support and immersing in a non-solvent, an alcohol, to quickly precipitate the polymer. The phase inversion technique could usually result in zwitterionic copolymer selective layers with thickness between 1 and 1.2 μm [27].

This process was a modified version NIPS that is very commonly used in laboratory preparation of membranes [29,30]. Unfortunately, NIPS is challenging to control at a laboratory scale a and has the added drawback of relegating most of the material to the support layer where it serves no functional purposes in providing selectivity (we refer to these membranes as integrated asymmetric membranes). As we develop new materials with unique properties, especially those that might be expensive to make, we may want to limit the use of those materials only to that part of the membrane where their use is justified. The TFC platform seems to be a better approach to minimizing the use of exotic materials in membrane selective layers. Unfortunately, few options exist to form these new materials through an *in-situ* approach such as interfacial polymerization.

That has not stopped some from trying. Techniques like spin coating [31] or dip coating [32] of the polymer solution onto a porous support were reported to make polymeric TFC membranes with reasonable permeance and rejection, but these techniques are inherently batch processes and not scalable. For example, Hall et al. [33] demonstrated that spin coating can make membranes thinner than 100 nm, but it is not a scalable process and often lacks control. Other additive approaches, like atomic layer deposition [34,35] or layer-by-layer deposition [36], are largely experimental techniques relegated to the laboratory to produce small membrane areas. Making ultra-thin films (less than 0.5 μm in thickness) by conventional casting has remained elusive.

Additive manufacturing has been explored in membrane fabrication such as oil-water separation membranes [37], thin film composite membranes [38], mixed matrix membranes [39] and ion exchange membranes [40]. Previous studies have demonstrated the ability of additive manufacturing in forming ultra-thin (sub-100 nm) polyamide RO and NF selective layer with enhanced permeance [38,41,42]. The purpose of this work is to present a recently developed additive manufacturing process for making TFC membranes with zwitterionic copolymer selective layers. These selective layers are intended to be homogenous, isotropic, and far thinner than those attainable with conventional casting. During electrospray, a high voltage is applied to a solution being extruded from a small needle and the Coulombic forces overcome the surface tension and create a fine spray which can lead to exceedingly thin film formation with controllable thickness. This technique was applied in this work to create thin film composite membranes by expanding upon the work by Bengani and Asatekin by using the PTFEMA-*r*-SBMA zwitterionic copolymers. The novelty of this work lies in its ability to form thickness controllable selective layers displaying exceptionally higher permeance without loss of selectivity for some organic molecules compared to those membranes made by NIPS.

2. Materials and methods

2.1. Materials

PTFEMA-*r*-SBMA (36 wt% SBMA in copolymer) was synthesized by the Asatekin lab (Tufts University, Medford, MA) using techniques described elsewhere [26]. Isopropanol, trifluoroethanol and dimethylformamide were purchased from Sigma Aldrich (St. Louise, MO). PAN 400 ultrafiltration membranes were purchased from Sepro Membranes (Oceanside, CA) and Sterlitech Corporation (Kent, WA) and were used as support layer. Nonwoven polyester fabric was purchased from Ahlstrom (Helsinki, Finland) and used as mechanical support for the TFC membrane. Deionized water was produced by and was used for all experiments. Methyl Orange (MO, 327 Da, Thermo Fisher Scientific), Vitamin B2 (VB2, 376 Da, Sigma Aldrich), Acid Fuchsin (AF, 585 Da, Acros Organics), Chlorophyllin Sodium Copper Salt (CP, 724 Da, Santa Cruz Biotechnology, Inc.), Vitamin B12 (VB12, Thermo Fisher Scientific) and Brilliant Blue R (BLBR, Sigma Aldrich) were used as dyes for rejection tests. All materials were used as-received.

2.2. Synthesis of zwitterionic copolymer

The copolymer was synthesized using methods described in previous work [26–28], as indicated in Fig. 1. 12 g of sulfobetaine methacrylate (SBMA), 18 g of trifluoroethyl methacrylate (TFEMA), 0.30 g of lithium chloride, and 0.030 g of Azobisisobutyronitrile (AIBN) were first dissolved in 240 mL of dimethyl sulfoxide (DMSO). Next, the reaction flask was sealed with a rubber septum, purged with nitrogen for 20 min, and immersed in a 70 °C oil bath. The reaction was terminated after 20 hours by adding 1.5 g of 4-methoxyphenol. The copolymer was then precipitated in 2400 mL of a mixture of ethanol and hexane (50:50 vol ratios) and washed several times with ethanol. Afterwards, the copolymer was aerially dried for several days and then dried an additional 24 hours at 50 °C under vacuum. Composition of 35.5 wt% SBMA and 64.5 wt% TFEMA was determined by H NMR spectroscopy (Fig. 2). Based on previous research conducted by Bengani et al. [27], the molecular weight of this zwitterionic copolymer was characterized by dynamic light scattering (DLS) as 1.19×10^6 g/mol. The glass transition temperature was measured by differential scanning calorimetry (DSC) to be

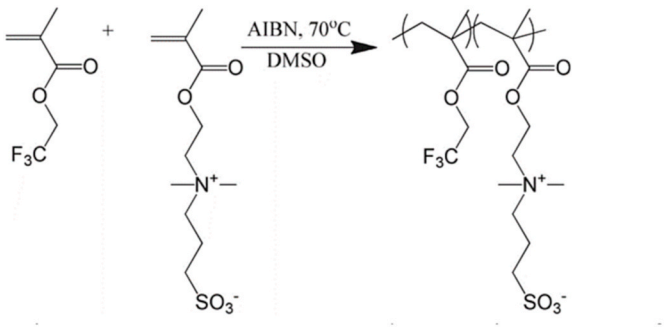

Fig. 1. The reaction between two monomers: SBMA and TFEMA. This reaction is a free radical polymerization which results in a random copolymer [26].

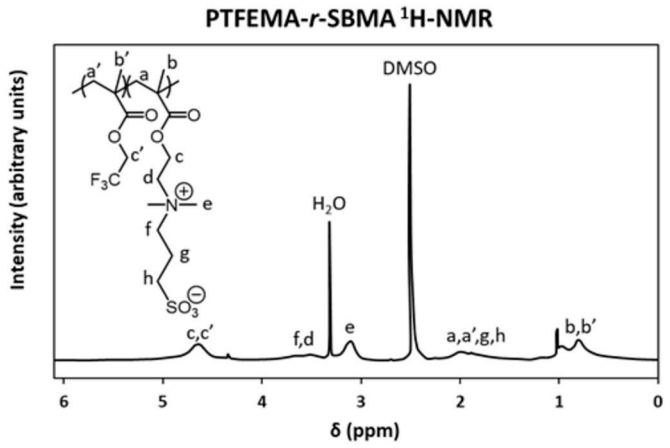

Fig. 2. NMR of PTFEMA-*r*-SBMA. A content of 35.5 wt% SBMA and 64.5 wt% TFEMA was found for the copolymer based on NMR result.

173 °C [27]. The bicontinuous network of the zwitterion nanochannels and the TFEMA phases were also illustrated in the TEM images of their previous work [27]. The structure and properties of cast PTFEMA-*r*-SBMA membrane has been studied by Bengani in her previous papers [26–28].

2.3. Membrane fabrication

The membrane fabrication process is illustrated in Fig. 3. The solutions were prepared by dissolving the synthesized zwitterionic copolymer PTFEMA-*r*-SBMA in mixed solvent (TFE: DMF = 1: 1 v/v) in a 50 °C water bath. The copolymer is comprised of 36 wt% SBMA, which was shown in previous studies to lead to membranes with good rejection and fouling resistance [26]. Polymer solution concentration was varied from 0.001% w/v to 1% w/v (Table 2). The printing device is illustrated in Fig. 3 and described in detail elsewhere [38]. The copolymer solution and a nonsolvent were sequentially sprayed using positively charged needles held in place holder that was rastered by a screw-driven slide (Velmex), which moved along the rotating drum's axis. Bengani et al. have demonstrated in their previous paper [26] that cast membranes were immersed in IPA nonsolvent bath for phase inversion. Therefore, in this work the nonsolvent IPA was also deposited on the substrate to precipitate the copolymer from the solution. The PAN400 ultrafiltration membrane was wrapped on the drum to serve as a substrate for the thin film. The needle tips were connected to a high–voltage direct current power source that could generate voltage between 0 and 30 kV. The

Table 1
Dyes used and their molecular weight, size, charge and absorbance wavelength [26].

Dye	Molecular Weight (g/mol)	Calculated size (Å)	Charge
Methyl Orange	327.3	7.94	−1
Vitamin B2	376.36	8.49	0
Acid Fuchsin	580	9.27	−2
Brilliant Blue R	825.97	11.08	−1
Chlorophyllin Sodium Copper Salt*	724.15	11.5	−5
Vitamin B12	1355.37	13.14	0

* The dissociation of chlorophyllin salt in water has not been well studied. Here it is assumed that the chlorophyllin salt fully dissociates in water and carries 5 negative charges. The size of each dye molecule was calculated based on the molecular volume computed by Molecular Modeling Pro.

Table 2
Calculated selective layer thicknesses (Unit: nm) prepared using solutions with various polymer concentrations.

Concentration (% w/v)	Thickness (5 layers) (nm)	Thickness (10 layers) (nm)
0.001	0.36*	0.73*
0.01	3.64*	7.28*
0.0625	22.73	45.46
0.2	72.73	145.47
0.3	109.1	218.2
0.4	145.47	290.94
0.5	181.83	363.37
1.0	363.37	727.34

* These thicknesses were only calculated and not measured with SEM since they were too thin to be detected in images. The actual thicknesses of these thin selective layers were extrapolated from the calibration curve in Fig. 5.

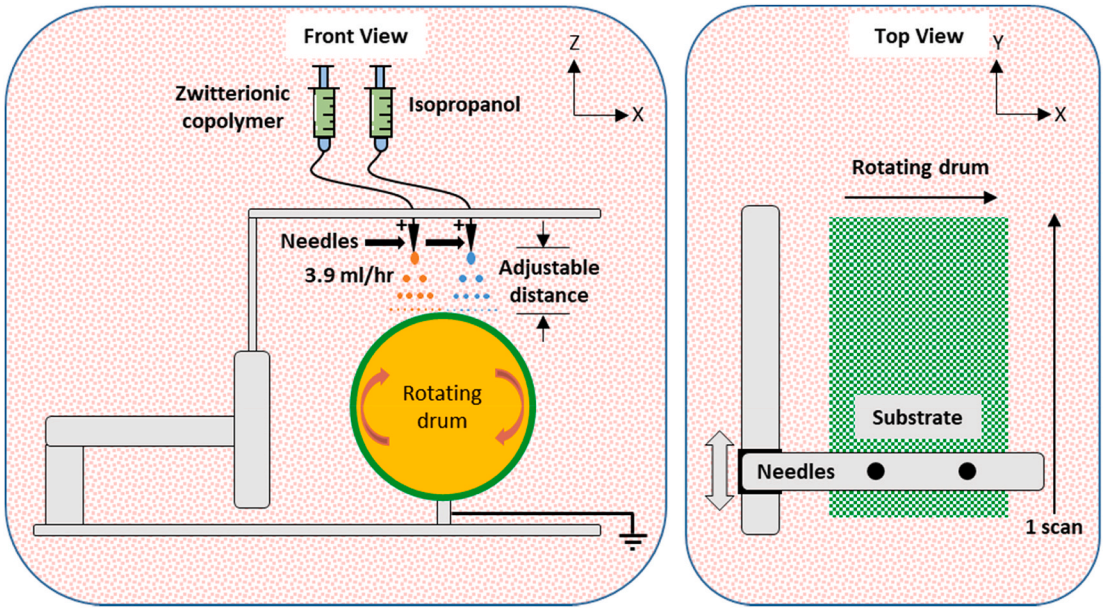

Fig. 3. A schematic diagram of the membrane fabrication process. The electrospray system is enclosed and ventilated (not shown). The polymer solution was prepared by dissolving the synthesized copolymer in mixed solvent (TFE: DMF = 1: 1 v/v) in a 50 °C water bath. To anneal the membranes, they were soaked in a 50 °C water bath for 2hrs after electrospray. The membranes were subsequently stored in DI water for filtration tests.

voltage applied on the needle tips was adjusted between 11 and 12 kV in order to establish a desirable spray pattern. The tip-to-drum distance was kept between 4 and 5 cm. Membranes were formed at 23 °C and 16% RH [43]. By extruding both the polymer solution and the non-solvent out of the positively charged needle tips at a fixed flow rate of 3.9 mL/hr, cone-and-jet spray patterns composed of copolymer solution and IPA aerosols were formed, which subsequently led to two individual circular deposition areas on the substrate. The Velmex movement along the drum axial direction was subsequently initialized and carried the needles to scan above the entire rotating substrate area. One printing layer is defined as a single pass over the drum surface. Membranes were made with 5 or 10 layers with both the polymer solution and IPA being deposited. Selective layer thickness was varied by adjusting the polymer solution concentration and the number of layers deposited. Based on the self-assembly mechanism demonstrated by Bengani et al. in their previous paper [26], the PTFEMA-*r*-SBMA copolymer self-assembled into a bicontinuous network composed of zwitterionic nanochannels and hydrophobic domains during the phase inversion after the solvent evaporated. The self-assembly was due to the dipole-dipole affinity between the zwitterion pairs and the difference in Flory-Huggins parameter (χ) between the hydrophobic copolymer segment and the zwitterion segment. This happens regardless of the type of solution processing we use. Therefore, during the electrospray process, the self–assembled structure formed when phase inversion took place after both copolymer solution and IPA were deposited on the membrane support.

2.4. Membrane annealing

Annealing is able to improve the conformational motion of polymer chains, which results in a more interconnected self-assembled copolymer selective layer. Therefore, thicker selective layers after annealing were composed of nanochannels with better continuity and connectivity, which resulted in higher permeance value. The enhancement of self-assembly by thermal annealing was also reported in other research. Guarini et al. [44] studied the effect of annealing on PS/PMMA block copolymer thin film and proposed that annealing was able to narrow pore size distribution of self-assembled diblock copolymer and form a more organized self-assembled structure. Black et al. [45] demonstrated that annealing was able to effectuate phase separation between different polymeric block components contained in the block copolymer. As shown in Fig. 3, membranes were annealed in a water bath for 2 hours at 50 °C before being immersed in DI water overnight prior to filtration tests.

2.5. Selective layer thickness calculation

Selective layer thickness was varied by adjusting the polymer solution concentration and the number of layers and was calculated based on material mass balance:

$$\delta_{theoretical} = \frac{m_{polymer}}{\rho_{polymer} \times A} \tag{1}$$

$$m_{polymer} = N \times V_0 \times C \tag{2}$$

$$\rho_{polymer} = \frac{1}{\frac{\omega_{PSBMA}}{\rho_{PSBMA}} + \frac{\omega_{PTFEMA}}{\rho_{PTFEMA}}} \tag{3}$$

In these equations, A is the spray area (cm^2), N is the printing layer number, V_0 is the volume of the polymer solution ejected per printing layer, C is the polymer solution concentration (w/v), $\rho_{polymer}$ is the density of the copolymer, ρ_{PTFEMA} [46] and ρ_{PSBMA} [47,48] are the densities of the homopolymers, ω_{PTFEMA} and ω_{PSBMA} are the mass fractions of the homopolymers and $m_{polymer}$ is the mass of the copolymer deposited on the substrate. Here volume additivity is hypothesized in the calculation of the copolymer density [49].

2.6. Membrane performance characterization

2.6.1. Water permeance and permeability

After printing, the TFC membrane was cut into a 75 mm diameter flat disc and placed on top of a non-woven supportive polyester fabric layer before being installed in a pressurized stirred cell (custom built) for testing. Tests were run in dead-end mode with N_2 gas providing a pressure of 20 psi. Deionized water was used for pure water permeance tests. Membranes were equilibrated for 30 min to allow for stabilization. After flux stabilization, permeate samples were collected and weighed every 15 min for an hour. Each data point is indicative of three independent membrane coupons tested in parallel at the same conditions. Pristine PAN400 control membranes were also tested at the same conditions for comparison.

Permeability is defined as thickness normalized permeance and can be calculated using equation (6), where selective layer permeability is the division of thickness by its resistance. Membrane rejection is defined in equation (7):

$$A = \frac{J}{\Delta p} = \frac{1}{R_{membrane}} \tag{4}$$

$$R_{membrane} = R_{selective} + R_{\text{support}} \tag{5}$$

$$P = A\delta = \frac{\delta}{R_{selective}} \tag{6}$$

$$R(\%) = \frac{C_f - C_p}{C_f} \times 100 \tag{7}$$

Where A is the water permeance (LMH/bar), J is the water flux (LMH), Δp is the *trans*-membrane pressure difference (bar). $R_{membrane}$ is the resistance of the TFC membrane (bar m^2 hr L^{-1}), $R_{selective}$ is the resistance of the selective layer (bar m^2 hr L^{-1}) and R_{support} is the resistance of the support layer (bar m^2 hr L^{-1}). P refers to the selective layer water permeability (L μm bar^{-1} $m^{-2}hr^{-1}$) and δ is the selective layer thickness (μm). R is the membrane rejection (%), C_f is the feed solution concentration (mg/L) and C_p is the permeate solution concentration (mg/L).

2.6.2. Dye rejection

Membrane rejection was measured with neutral and anionic dyes with varying molecular diameter. Table 1 shows the molecular weight, calculated molecular diameter and the charge of each dye used in this study. The calculated size of dye molecules was computed by first determining the molecular volume of each dye using Molecular Modeling Pro software and then determining the diameter of a sphere of equal volume. This value is likely an underestimate of the true hydrodynamic diameter of each dye, as it does not account for hydration. Nonetheless, it was found to closely and predictively correlate with the selectivity of membranes prepared from zwitterionic self-assembling copolymers including PTFEMA-*r*-SBMA [26]. Each dye was dissolved in DI water to form a 100 mg/L aqueous solution, which was subsequently filtered through the membranes in the dead-end cell system with continuous stirring to reduce fouling. Permeate was collected at 25 min intervals for the first 100 min. The concentration of the feed and the permeate dye solution was measured by UV–vis spectroscopy.

2.7. Characterization of selective layer thickness

Selective layer thickness was characterized by examining the cross-section morphology of the TFC membranes by using Phenom G2 Pure Tabletop Scanning electron microscopy (SEM) operating at 5 kV and at 19,000× magnification. In order to prepare a clean cross-section surface, TFC membranes were freeze fractured in liquid nitrogen, mounted, and sputter coated with Au/Pd.

3. Results and discussion

3.1. Selective layer thickness characterization

The thickness of the selective layers is presented in Table 2. The polymer solution concentration was varied from 0.001% w/v to 1.0% w/v and solutions were deposited in 5 and 10 layer increments. When the selective layer went down to sub-10 nm, the SEM could no longer detect the selective layer as these thicknesses exceeded the detection limit of SEM. Therefore, the thicknesses of these thin membranes could only be extrapolated from the correlation between SEM measured thickness and the calculated.

Cross-sectional SEM images (Fig. 4) of the TFC membranes also reveal the thickness of the selective layer, which can be directly compared with the calculated thickness. A parity plot showing the calculated thickness and cross-sectional thickness obtained from SEM imaging (Fig. 5) has a slope of ~1, which suggests that this method of "calibrating" thickness to be appropriate. Table 2 shows the calculated data of the thickness across the membranes that were made. It is noted that the very thin membranes had thicknesses that were extrapolated from the calibration curve in Fig. 5(A). These thicknesses also do not account for the potential of intrusion of polymer into the support layer pores, which is more likely to happen with lower concentration polymers. The ratio of cross section thickness and calculated thickness at varying thicknesses (Fig. 5(B)) shows that for membranes whose selective layers were thinner than 100 nm, these two thicknesses are no longer consistent. SEM images also show that selective layers formed by 0.0625% w/v solution are indistinguishable from the skin layer of the support. Therefore, thickness measurement for extremely thin membranes is prone to error due to the possibility of the penetration of polymers into the pores and due to the difficulty to distinguish the selective layer from the support skin layer when using electron microscopy. We also note that SEM images are taken at high vacuum, which may cause changes in the polymer structure and bias in the measurements.

3.2. Water permeance

Fig. 6(A) and (B) shows water permeance values of the 5 and 10 layered membranes with increasing selective layer thickness. A commercial membrane (Sartorius, PES20) with similar pore size to these membranes is included as a control [26]. Since water permeance is inversely proportional to selective layer thickness, a decrease of permeance with increasing membrane selective layer thickness was expected and observed. The 0–10 LMH/bar region of Fig. 6(A) was magnified in Fig. 6(B) to improve fidelity of the data for analysis. Interestingly, similar water permeance values were observed between membranes with the same selective layer thickness achieved by varying printing layers and solute concentration. For example, the membrane produced with 5 layers of a 1.0% w/v polymer solution had a calculated thickness of 364 nm and exhibited a permeance of 2.0 LMH/bar. A membrane made with 10 layers of a 0.5% w/v polymer solution also had the same thickness and had a measured permeance of 1.9 LMH/bar. When membrane thickness was reduced to around 100–200 nm, a similar permeance to previously reported solvent-cast membranes [26] was achieved. As the membrane thickness was further reduced, permeance increased substantially with our most permeable membranes exhibiting permeance that was indistinguishable from the support layer. It is also noted that water permeance remains constant when the selective layer is thicker than 300 nm. We hypothesize that there may be asymmetry in these thicker layers since we are using a non-solvent to precipitate them. If this is the case, then the permeance would be dictated by a skin layer within this printed layer and not by the full layer thickness. We see no evidence of asymmetry within the printed layer,

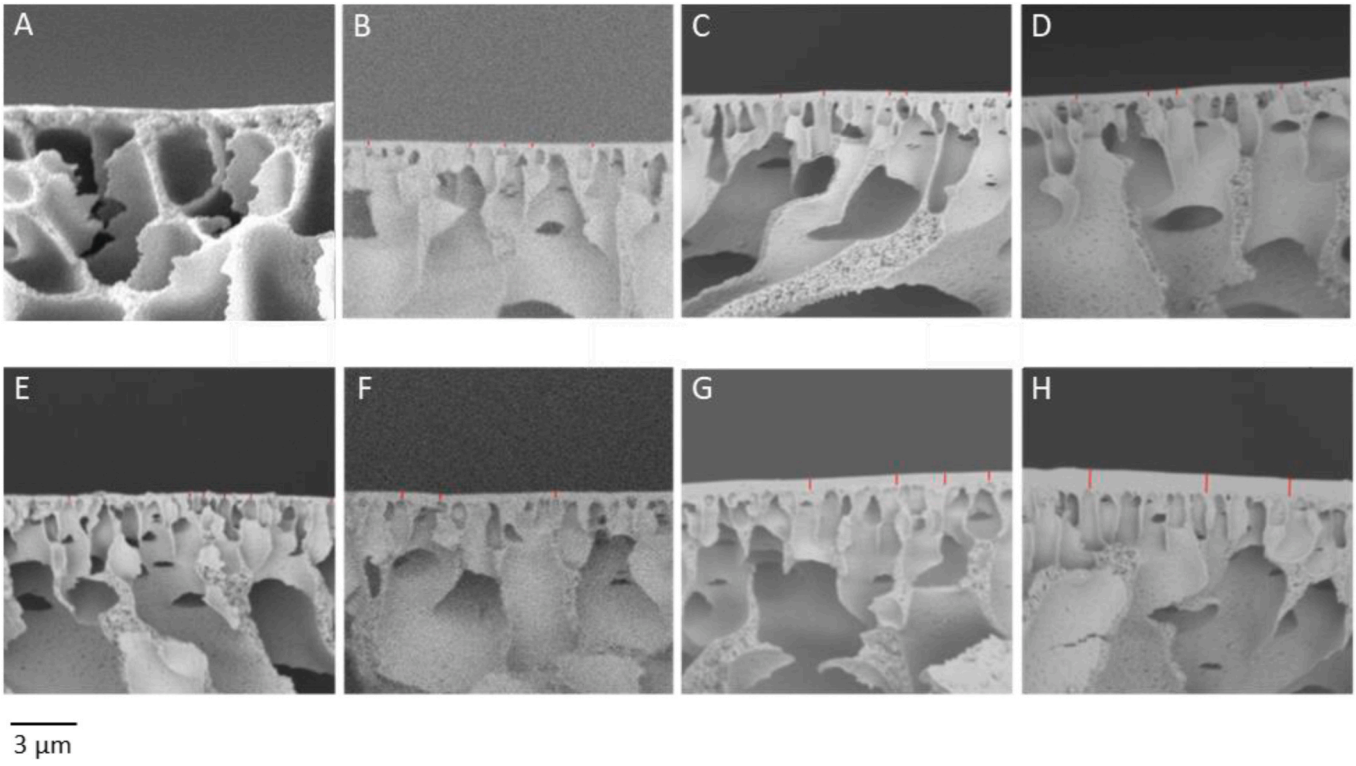

Fig. 4. Cross section SEM images of printed TFC membrane with varying printing layers and copolymer solution concentration. Support layer cross section image is taken as control. Selective layer thickness is directly measured on the cross section image. (A) Uncoated support layer. (B–D) TFC membranes printed with 5 printing layers of (B) 0.0625% w/v (C) 0.3% w/v (D) 0.4% w/v copolymer solution. (E–H) TFC membranes printed with 10 printing layers of (E) 0.0625% w/v (F) 0.3% w/v (G) 0.5% w/v (H) 1.0% w/v copolymer solution. Please note that this figure is best viewed in color. (For interpretation of the references to color in this figure legend, the reader is referred to the Web version of this article.)

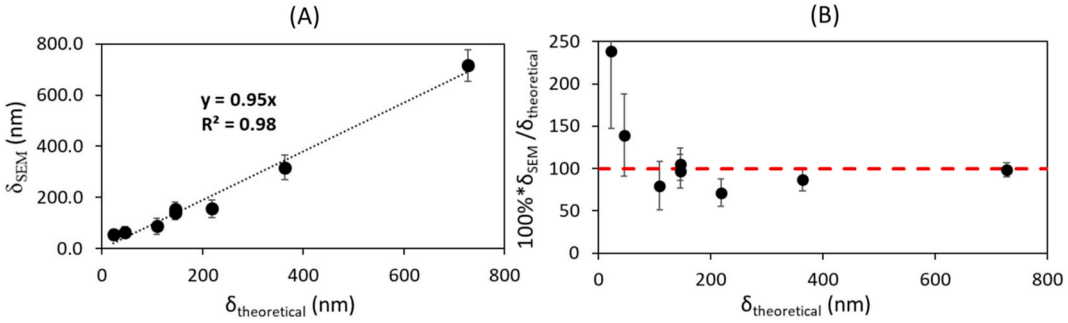

Fig. 5. (A). Relationship between calculated thickness and cross section thickness. (B). Ratio of cross section thickness and calculated thickness at varying selective layer thickness. Calculated (theoretical) thickness: thickness calculated based on mass balance of copolymer solute. Cross section thickness: thickness measured based on cross section SEM images. Please note that this figure is best viewed in color. (For interpretation of the references to color in this figure legend, the reader is referred to the Web version of this article.)

but such a result would be consistent with phase inversion casing membranes with skin layers of 1 μm or more.

Fig. 6(C) shows water permeability as it relates to selective layer thickness. The calculation of permeability is based on resistance-in-series model which was mentioned in 2.5.1. The resistance of the support was removed during the calculation so the permeability of the selective layers are presented here. Since permeability is an intrinsic property of the polymer, this should be independent of thickness. However, a deviation in that behavior was noted when the membrane selective layer thickness is less than 100 nm. Some of this deviation is due to the lack of accuracy in calculating thickness under 100 nm. However, this deviation is believed to be caused by interlayer spacing between each layer. Spacing between layers, which was noted at times in our previous work with polyamide membranes [38], may serve as "highways" for water to transport between layers in order to find the next layer's pore opening. We believe these interlayer highways are potentially caused by air trapped between two polymer layers. The effect is most noted for the membranes with fewer layers, where a defect in a single layer would have a greater impact on permeance and may artificially inflate a permeability calculation.

This is particularly noted given the fact that membrane selective layers above 100 nm in thickness exhibited a consistent water permeability value of 0.89 LMH/bar*μm while it increases significantly at lower thicknesses. This may be an artifact of the deviation from linearity in the thickness measurement parity plot in Fig. 5(B) since our ability to measure thickness below 50 nm is limited. It may also have to do with the "highways" present in the multi-layered films. If the layers are individually very thin, a defect in a single layer is more likely, though that defect is unlikely to occur in the same location as the next layer. A defect is likely to give water a rapid transport pathway to the next layer, where the highway between the layers can facilitate transport to the defect or to the next available hydrophilic region in the polymer. This is supported by Fig. 6(C) given that the permeabilities of the 10-layer membranes are higher than the 5-layer membranes (for membranes of the same overall thickness). This means the individual layers of the 10 layer membranes are half as thick and therefore more susceptible to bypass by a defect, leading to a higher than expected permeability calculation for a given thickness.

As a comparison, polyamide NF membranes have been reported with thicknesses as low as 145 nm with permeability of 2.05 LMH/bar*μm [50]. A recent report from our lab on printed polyamide RO membranes produced through this method yielded a permeability value of 0.14 LMH/bar*μm [38]. Our membranes made with a thickness of 45.46 nm and 72.73 nm closely with the permeability value of NF membranes. Membranes thinner than 45.46 nm even show a higher permeability while membranes thicker than 100 nm exhibit permeability values between RO and NF.

Annealing membranes in warm water (Fig. 6(D)) was found to increase permeance for each of our membranes tested, especially for thicker membranes. This result was further supported by the comparison on water contact angle of annealed and unannealed membranes, as indicated in the supplementary material. Based on the discussion in section 2.3, annealing is thought to help bridge the hydrophilic channels in sequential layers by allowing the self-assembled structures to align better between layers and get interconnected. The greater impact on thicker membranes is due to the importance of inter-layer alignment of the self-assembly for membranes with either thicker or greater numbers of layers. Annealed membranes printed with 1% w/v copolymer solution exhibited almost 3.4 (5 layers) and 4.7 (10 layers) times higher stabilized water permeance than membranes without annealing. It is noted that even our thickest membranes exhibited a 64% higher permeance than the cast membranes after annealing.

3.3. Dye rejection

Dyes with a variety of sizes and charges were used to characterize the rejection of TFC membranes with all selective layer thicknesses. These are presented below as stabilized rejection. Stabilization data can be found in the supplementary materials.

3.3.1. Chlorophyllin rejection

Fig. 7 shows the chlorophyllin rejection for membranes with different thickness. It is noticed that these membranes exhibited almost a complete rejection of the dye, presumably due to its high charge (−5). The negative charge results in substantial charged-based exclusion from the membrane. The charge also contributes to hydration of the molecule, increasing the effective molecular size of the chlorophyllin. To ensure that the high rejection was not caused by the support layer, control experiments were run with the as-received support layer and the support layer after "printing" only the solvent (with no polymer). Our results indicate that the support layer did have intrinsic rejection of chlorophyllin of 75–80% and that this rejection was not changed appreciably by the exposure of the support membrane to the solvent used to deposit the zwitterionic copolymer. The deposition of even the most dilute polymer solution resulted in complete rejection of chlorophyllin. It is hypothesized here that when printing the most dilute copolymer solutions, the layer of the copolymer on the membrane is too thin to see in a SEM image yet still blocks pores in a way that dramatically increases selectivity. Additionally, it is also noticeable that annealing greatly improved the membrane permeance (as discussed in Fig. 6(D)) and did not impact the chlorophyllin rejection of any membrane printed with zwitterionic copolymer. This data was remarkable as it shows that even the thinnest layer of the polymer results in remarkable rejection of charged compounds without loss of water permeance (Fig. 6(A)).

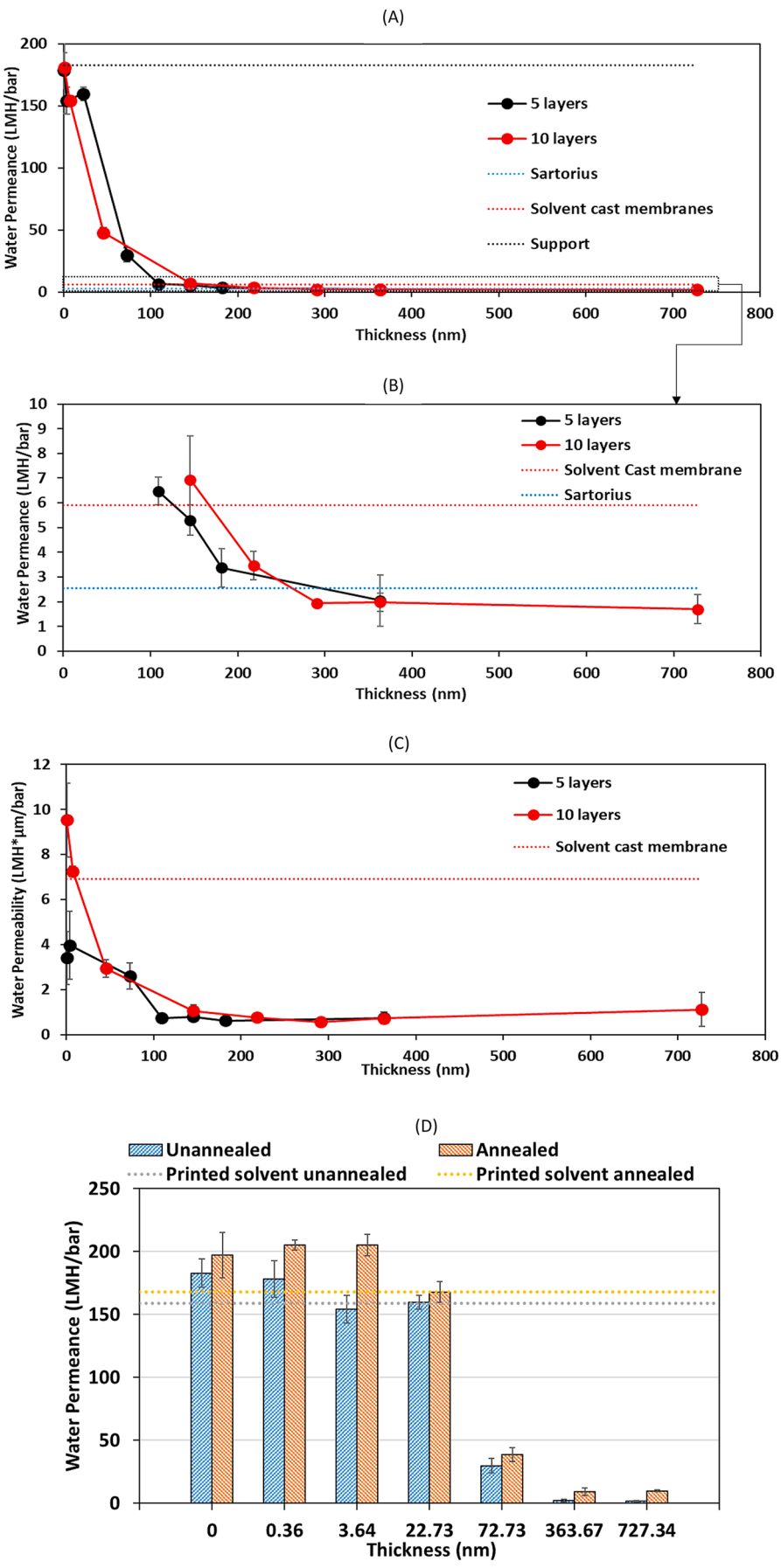

Fig. 6. (A) Comparison of water permeance between TFC membranes with various selective layer thickness (both 5 and 10 layers), cast TFC membranes (red dashed line) and commercial PES1 (1 kDa cutoff) membrane (green dashed line). (B) Magnified graph of water permeance change with respect to increasing selective layer thickness. Membranes with the same thickness but different printing layers show similar water permeance. (C). Selective layer water permeability with increasing thickness. Please note that this figure is best viewed in color. (D). Water permeance of pre and post-annealed membranes. (For interpretation of the references to color in this figure legend, the reader is referred to the Web version of this article.)

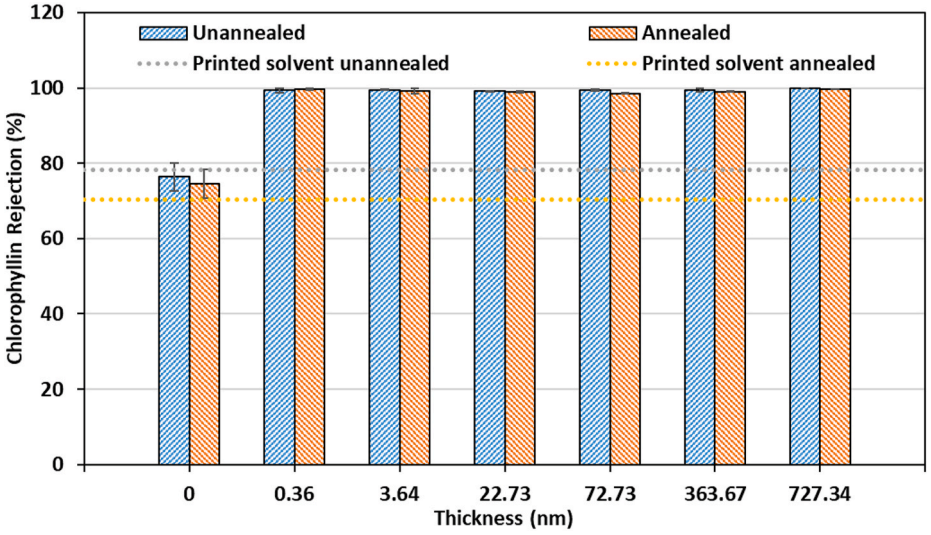

Fig. 7. Chlorophyllin rejection of TFC membranes with increasing selective layer loading. All topped with 5-layer copolymer solution. Please note that this figure is best viewed in color. (For interpretation of the references to color in this figure legend, the reader is referred to the Web version of this article.)

3.3.2. *Acid fuchsin rejection*

The rejection for acid fuchsin, which is a smaller molecule with lower charge (Fig. 8), was also tested to indicate the selectivity of the printed membranes. The thinnest membrane selective layers (which were around 20 nm) exhibited low rejection (less than 10%). Rejection was improved as the thickness increased to 100 nm and continued to rise to 83% above that thickness at 727 nm. The lower rejections at lower thicknesses were attributed to the prevalence of imperfections (they are not referred as "defects", as there is still reasonable rejection to indicate that large holes are not present). However, it is described above that the presence of individual layer imperfections that give rise to higher than expected permeability at low thickness may be further supported by this data. As thickness increases through addition of layers, the imperfections are blocked or filled in and selectivity improves. This is especially noticeable for smaller molecules. It was observed here that selective layers with the same thickness could yield similar acid fuchsin rejection regardless of the printing layers and dope solution recipe.

3.3.3. *Vitamin B12 rejection*

To control for charge effects on rejection, the relatively large vitamin B12 molecule (0 charge with molecular diameter of 1.314 nm) was selected. Similar to acid fuchsin, a similar sharp increase in rejection was measured as the thickness of the membrane reached 100 nm and exhibited maximum rejection of 92%. This rejection was notably higher than the acid fuchsin rejection given the size of the B12 molecule. Without charge, size exclusion was deemed the dominant mechanism for rejection in this case. Unlike acid fuchsin, there is negligible rejection difference at 50 nm membrane thickness between 5 and 10 layer membranes. This suggests that charge increases resistances to membrane transport, particularly with membranes with more layers of polymer. Fig. 9.

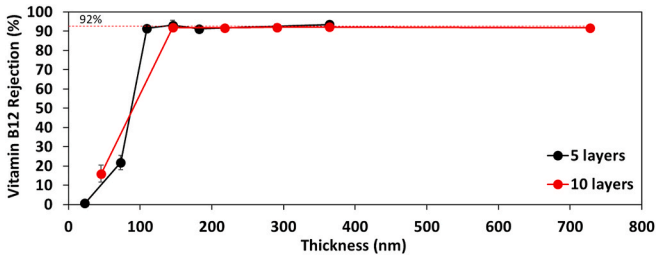

Fig. 9. Vitamin B12 rejection of TFC membranes with various selective layer thickness. Please note that this figure is best viewed in color. (For interpretation of the references to color in this figure legend, the reader is referred to the Web version of this article.)

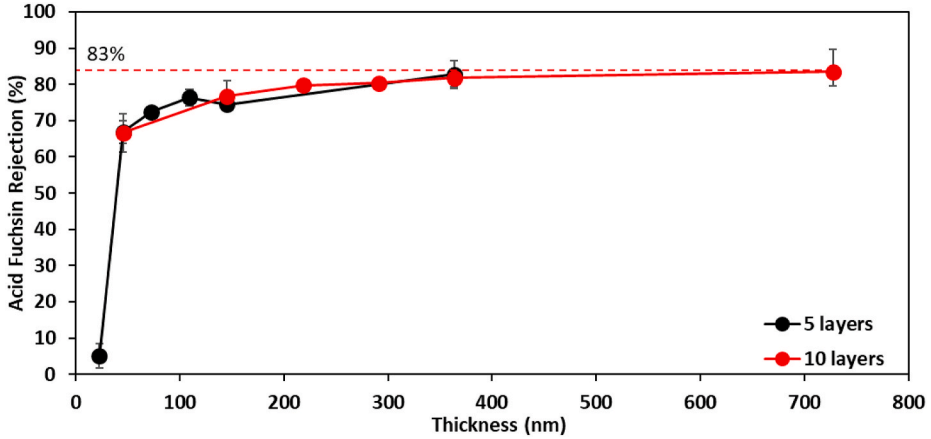

Fig. 8. Acid fuchsin rejection of TFC membranes with various selective layer thickness. Please note that this figure is best viewed in color. (For interpretation of the references to color in this figure legend, the reader is referred to the Web version of this article.)

3.3.4. Comparison of rejection to solvent-cast membranes

These particular dyes were chosen for comparison to data published on cast membranes [26]. Fig. 10 below is a "S-curve" showing stabilized rejections of our membranes relative to those published in the literature. The S-curve was fitted by donnan steric pore model (DSPM) based on the dye molecule diameters calculated by Molecular Modeling Pro (Table S1). The DSPM model and fitting procedure are presented in Supplementary Material. In this particular comparison, there are a mixture of charged and uncharged molecules across the molecule sizes, so this is not a true MWCO or size exclusion analysis, but this graph is shown here for comparison purposes only. The authors would like to comment that DSPM is used for estimating neutral dye rejection since the impact of dye charge on flux calculation the effect of hydration are not considered in this model. Therefore, this model cannot provide accurate prediction on the rejection of the dyes smaller than the size cutoff due to the abundance of charged dyes in that size range. However, this model is reasonably accurate for predicting rejection large than size cutoff and our printed membranes. For neutral dyes such as vitamin B2 and vitamin B12, all membranes showed a slightly lower rejection than a smaller charged dye. Compared with cast membranes, the printed membranes after annealing exhibit higher permeance while still maintaining an approximately 1.1 nm size cutoff.

The authors would also comment that dyes are not ideal for measuring cutoff as they differ in more than just size. Their charge, functionality, and shape will also impact selectivity. They were used due to the ease at which they are detected and measured. In general, if one uses dyes to measure selectivity, many dyes should be chosen in a way that controls for shape, charge, and size. We have chosen a small subset of dyes that provide the necessary data to demonstrate the selectivity of our high permeance NF membranes. A more comprehensive study with more dyes is beyond the scope of this work.

3.4. Membrane selectivity in binary dye solution

One beneficial feature of using dyes as selectivity markers is the ability to use mixtures of dyes to understand how selectivity can be impacted by the presence of other molecules. Dyes with the same charge and different diameters were mixed at 1:1 w/w to form a binary solution. Membrane selectivity was measured subsequently by the absorbance curve. Rejection values were calculated based on the absorbance value at the peak of the UV spectrum of each dye. Absorbance wavelengths were selected to limit interference between the two dyes. The absorbance curve for a charged dye mixture (methyl orange-brilliant blue R) is illustrated in Fig. 11(A). The absorbance curve indicates a 74% methyl orange rejection and a 96% rejection of brilliant blue R. This result shows that while maintaining the same charge, membranes were partially rejecting the smaller dye and virtually rejecting all the larger dye. As calculated in Fig. 11(C), the rejection of smaller dye in a mixture is much higher than the rejection obtained when testing rejection by itself (see SM). This is an indication of a synergistic effect in the binary mixture as the bigger brilliant blue R molecules might block the zwitterion channels and hinder methyl orange transport.

In order to characterize the size-based rejection for neutral dyes, a mixture of vitamin B2-vitamin B12 was prepared using the same concentrations. Since there is an overlap of two characteristic peaks at 360 nm, the rejection of vitamin B12 was calculated based on its tertiary peak at 555 nm. While this reduces the resolution of the measurement, it is not prone to interferences from other absorption spectra. The permeate curve in Fig. 11(B) reveals a near complete rejection of vitamin B12 and a partial rejection of vitamin B2. Interestingly, unlike with the charged dyes, the B2 rejection is not increased by the presence of the larger dye. This might mean that the same "ripening" phenomena, which may be a charge-driven effect with the binary dye test with brilliant blue and methyl orange, does not impact dye rejection for uncharged molecules that are selected by size.

4. Conclusion

This work demonstrates the 3D printing of zwitterionic copolymer NF membranes with exceptional performance. The electrospray printing technique enables fabrication of a TFC selective layer with controllable thickness below 50 nm, which is impossible to achieve for conventional polymer processing methods such as casting. Our best performing membranes exhibited water permeance up to 180 LMH/bar, which could be further improved to over 200 LMH/bar through annealing, with nearly complete rejection of chlorophyllin dye. The effect was more muted for smaller dyes like acid fuchsin or uncharged dyes like vitamin B12 as these dyes required a membrane thickness of at least 100 nm to achieve their maximum stabilized rejection. One of the more interesting findings of this work was that the intrinsic material's water permeability, which is calculable given that we know the membrane thickness, was much higher for thinner membranes. This result is attributed to interlayer imperfections within the thin film, which enabled water to bypass some layers. This bypassing did effect rejection for the smallest or least charged molecules tested. Similar to the cutoff value illustrated on cast membranes [26], the donnan steric pore model indicated a size cutoff of 1.1 nm for both annealed and unannealed printed membranes. This study also demonstrated the size based selectivity of printed membranes on both charged and neutral binary dye mixtures, together with a strong synergistic effect in the rejection of smaller dye in the negatively charged binary selectivity experiment.

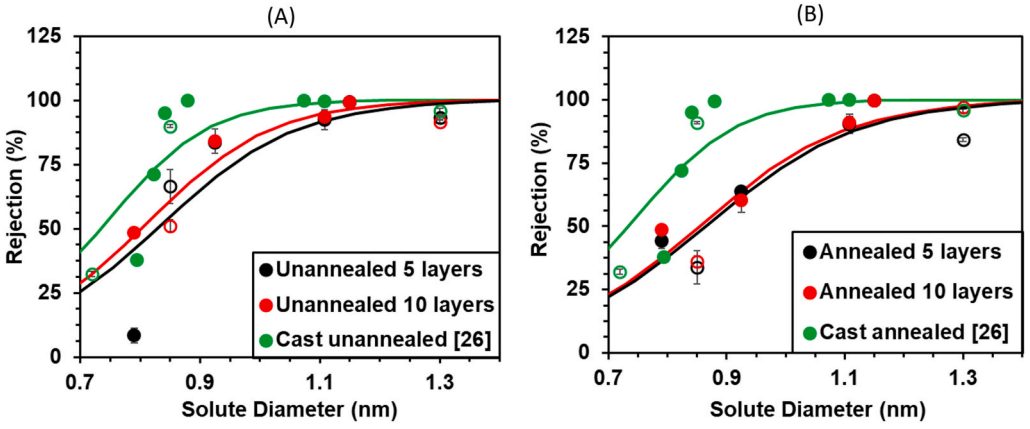

Fig. 10. Sized based dye rejection of TFC membranes with pre (A) and post (B) annealed membranes. Comparisons are made between the printed membranes and the cast membranes made by Bengani et al. [26]. Hollow data points represent neutral dyes and filled data points represent charged dyes. Please note that this figure is best viewed in color. (For interpretation of the references to color in this figure legend, the reader is referred to the Web version of this article.)

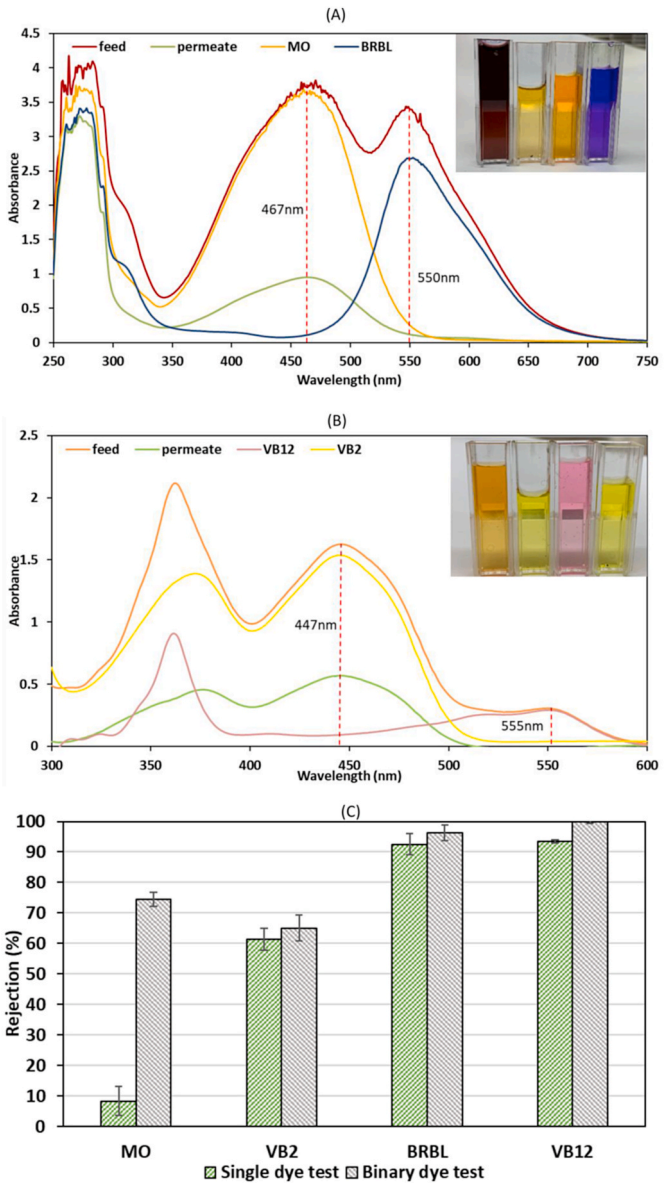

Fig. 11. (A). Absorbance curve of methyl orange-brilliant blue R binary mixture. Vials in the picture from left to right: feed (50 ppm MO with 50 ppm BRBL), permeate, 50 ppm MO, 50 ppm BRBL. All the dyes were dissolved in DI water. Instantaneous permeate was collected by filtering feed solution through 1% g/ml, 5-layer membrane overnight. Rejection values were calculated based on the absorbance value at the peak of the UV spectrum of each dye. (B). Absorbance curve of vitamin B2-vitamin B12 binary mixture. Vials in the picture from left to right: feed (50 ppm VB2 with 50 ppm VB12), permeate, 50 ppm VB12, 50 ppm VB2. All the dyes were dissolved in DI water. Instantaneous permeate was collected by filtering feed solution through 1% g/ml, 5-layer membrane overnight. (C). Comparison on rejection of all the 4 dyes in single and binary selectivity tests. (For interpretation of the references to color in this figure legend, the reader is referred to the Web version of this article.)

CRediT authorship contribution statement

Xin Qian: Conceptualization, Methodology, Formal analysis, Investigation, Data curation, Visualization, Writing – original draft. **Tulasi Ravindran:** Methodology, Investigation, Writing – review & editing. **Samuel J. Lounder:** Methodology, Formal analysis, Visualization, Writing – review & editing. **Ayse Asatekin:** Resources, Writing – review & editing, Project administration, Funding acquisition. **Jeffrey R. McCutcheon:** Conceptualization, Data curation, Supervision, Visualization, Writing – review & editing, Project administration, Funding acquisition.

Declaration of competing interest

The authors declare that they have no known competing financial interests or personal relationships that could have appeared to influence the work reported in this paper.

Acknowledgements

We acknowledge Zhenze Wu who provided assistance with testing. Funding was provided in part by the UConn Department of Chemical & Biomolecular Engineering, the UConn Academic Plan Internal Funding Program, the Fraunhofer USA Center for Energy Innovation, NSF CBET #1553661, NSF CBET #1160069, and NSF CMMI #2001544.

Appendix A. Supplementary data

Supplementary data to this article can be found online at https://doi.org/10.1016/j.memsci.2021.119428.

References

[1] B. Van Der Bruggen, C. Vandecasteele, T. Van Gestel, W. Doyenb, R. Leysenb, A review of pressure-driven membrane processes, Environ. Prog. 22 (1) (2003) 46–56.
[2] B. Nicolaisen, Developments in membrane technology for water treatment, Desalination 153 (1–3) (2003) 355–360, https://doi.org/10.1016/S0011-9164(02)01127-X.
[3] M.A. Shannon, P.W. Bohn, M. Elimelech, J.G. Georgiadis, B.J. Mariñas, A. M. Mayes, Science and technology for water purification in the coming decades, Nature 452 (2008) 301–310.
[4] E. Drioli, L. Giorno, E. Fontananova, Comprehensive Membrane Science and Engineering, 2010.
[5] Y.L. Ji, B.X. Gu, Q.F. An, C.J. Gao, Recent advances in the fabrication of membranes containing 'ion pairs' for nanofiltration processes, Polymers 9 (12) (2017) 1–49, https://doi.org/10.3390/polym9120715.
[6] K.P. Lee, T.C. Arnot, D. Mattia, A review of reverse osmosis membrane materials for desalination-Development to date and future potential, J. Membr. Sci. 370 (1–2) (2011) 1–22, https://doi.org/10.1016/j.memsci.2010.12.036.
[7] J.E. Cadotte, Evolution of composite reverse osmosis membranes, ACS Symp. Ser. (1985) 273–294, https://doi.org/10.1021/bk-1985-0269.ch012.
[8] H. Zhao, S. Qiu, L. Wu, L. Zhang, H. Chen, C. Gao, Improving the performance of polyamide reverse osmosis membrane by incorporation of modified multi-walled carbon nanotubes, J. Membr. Sci. 450 (2014) 249–256, https://doi.org/10.1016/j.memsci.2013.09.014.
[9] L. Xia, J. Ren, M. Weyd, J.R. McCutcheon, Ceramic-supported thin film composite membrane for organic solvent nanofiltration, J. Membr. Sci. 563 (2018) 857–863, https://doi.org/10.1016/j.memsci.2018.05.069.
[10] L. Xia, J.R. McCutcheon, Understanding the influence of solvents on the intrinsic properties and performance of polyamide thin film composite membranes, Separ. Purif. Technol. 238 (2020) 116398, https://doi.org/10.1016/j.seppur.2019.116398.
[11] S. Yu, M. Liu, X. Liu, C. Gao, Performance enhancement in interfacially synthesized thin-film composite polyamide-urethane reverse osmosis membrane for seawater desalination, J. Membr. Sci. 342 (1–2) (2009) 313–320, https://doi.org/10.1016/j.memsci.2009.07.003.
[12] J. Petersen, K.V. Peinemann, Novel polyamide composite membranes for gas separation prepared by interfacial polycondensation, J. Appl. Polym. Sci. 63 (12) (1997) 1557–1563, https://doi.org/10.1002/(SICI)1097-4628(19970321)63:12<1557::AID-APP6>3.0.
[13] Y. Song, J.B. Fan, S. Wang, Recent progress in interfacial polymerization, Mater. Chem. Front. 1 (6) (2017) 1028–1040, https://doi.org/10.1039/c6qm00325g.
[14] G.M. Whitesides, B. Grzybowski, Self-assembly at all scales, Science 295 (2002) 2418–2421.
[15] K.V. Peinemann, V. Abetz, P.F.W. Simon, Asymmetric superstructure formed in a block copolymer via phase separation, Nat. Mater. 6 (12) (2007) 992–996, https://doi.org/10.1038/nmat2038.
[16] A. Asatekin, C. Vannucci, Self-assembled polymer nanostructures for liquid filtration membranes: a review, Nanosci. Nanotechnol. Lett. 7 (2015) 21–32.
[17] Y. Zhang, N.E. Almodovar-Arbelo, J.L. Weidman, D.S. Corti, B.W. Boudouris, W. A. Phillip, Fit-for-purpose block polymer membranes molecularly engineered for water treatment, npj Clean Water 1 (1) (2018) 1–14, https://doi.org/10.1038/s41545-018-0002-1.
[18] S.P. Nunes, Block copolymer membranes for aqueous solution applications, Macromolecules 49 (8) (2016) 2905–2916, https://doi.org/10.1021/acs.macromol.5b02579.

[19] S.P. Nunes, A. Car, From charge-mosaic to micelle self-assembly: block copolymer membranes in the last 40 years, Ind. Eng. Chem. Res. 52 (3) (2013) 993–1003, https://doi.org/10.1021/ie202870y.
[20] S.P. Nunes, et al., Switchable pH-responsive polymeric membranes prepared via block copolymer micelle assembly, ACS Nano 5 (5) (2011) 3516–3522, https://doi.org/10.1021/nn200484v.
[21] S. Dami, C. Abetz, B. Fischer, M. Radjabian, P. Georgopanos, V. Abetz, A correlation between structural features of an amphiphilic diblock copolymer in solution and the structure of the porous surface in an integral asymmetric membrane, Polymer 126 (2017) 376–385, https://doi.org/10.1016/j.polymer.2017.05.024.
[22] S. Saleem, S. Rangou, C. Abetz, B. Lademann, V. Filiz, V. Abetz, Block copolymer membranes from polystyrene-b-poly(solketal methacrylate) (PS-b-PSMA) and amphiphilic polystyrene-b-poly(glyceryl methacrylate) (PS-b-PGMA), Polymers 9 (2017) 6, https://doi.org/10.3390/polym9060216.
[23] Z. Zhang, M.M. Rahman, C. Abetz, B. Bajer, J. Wang, V. Abetz, Quaternization of a polystyrene-block-poly(4-vinylpyridine) isoporous membrane: an approach to tune the pore size and the charge density, Macromol. Rapid Commun. 40 (3) (2019) 1–7, https://doi.org/10.1002/marc.201800729.
[24] M. Zhou, et al., New type of membrane material for water desalination based on a cross-linked bicontinuous cubic lyotropic liquid crystal assembly, J. Am. Chem. Soc. 129 (31) (2007) 9574–9575, https://doi.org/10.1021/ja073067w.
[25] G.S. Georgiev, et al., Self-assembly, antipolyelectrolyte effect, nonbiofouling properties of polyzwitterions, Biomacromolecules 7 (4) (2006) 1329–1334, https://doi.org/10.1021/bm050938q.
[26] P. Bengani, Y. Kou, A. Asatekin, Zwitterionic copolymer self-assembly for fouling resistant, high flux membranes with size-based small molecule selectivity, J. Membr. Sci. 493 (2015) 755–765, https://doi.org/10.1016/j.memsci.2015.07.025.
[27] P. Bengani-Lutz, E. Converse, P. Cebe, A. Asatekin, Self-assembling zwitterionic copolymers as membrane selective layers with excellent fouling resistance: effect of zwitterion chemistry, ACS Appl. Mater. Interfaces 9 (24) (2017) 20859–20872, https://doi.org/10.1021/acsami.7b04884.
[28] P. Bengani-Lutz, R.D. Zaf, P.Z. Culfaz-Emecen, A. Asatekin, Extremely fouling resistant zwitterionic copolymer membranes with ~ 1 nm pore size for treating municipal, oily and textile wastewater streams, J. Membr. Sci. 543 (2017) 184–194, https://doi.org/10.1016/j.memsci.2017.08.058.
[29] V.S. Sapkal, P.G. Bansod, Development of casting techniques for polyethersulfone ultra filtration membranes and their effects on flux and rejection, Int. J. Chem. Sci. Appl. 2 (2) (2011) 156–161.
[30] X.L. Li, L.P. Zhu, B.K. Zhu, Y.Y. Xu, High-flux and anti-fouling cellulose nanofiltration membranes prepared via phase inversion with ionic liquid as solvent, Separ. Purif. Technol. 83 (1) (2011) 66–73, https://doi.org/10.1016/j.seppur.2011.09.012.
[31] F. Shao, et al., Graphene oxide modified polyamide reverse osmosis membranes with enhanced chlorine resistance, J. Membr. Sci. 525 (2017) 9–17, https://doi.org/10.1016/j.memsci.2016.12.001.
[32] L. Ni, J. Meng, X. Li, Y. Zhang, Surface coating on the polyamide TFC RO membrane for chlorine resistance and antifouling performance improvement, J. Membr. Sci. 451 (2014) 205–215, https://doi.org/10.1016/j.memsci.2013.09.040.
[33] D.B. Hall, P. Underhill, J.M. Torkelson, Spin coating of thin and ultrathin polymer films, Polym. Eng. Sci. 38 (12) (1998) 2039–2045, https://doi.org/10.1201/9781315108292-33.
[34] R. Shang, A. Goulas, C.Y. Tang, X. de Frias Serra, L.C. Rietveld, S.G.J. Heijman, Atmospheric pressure atomic layer deposition for tight ceramic nanofiltration membranes: synthesis and application in water purification, J. Membr. Sci. 528 (2017) 163–170, https://doi.org/10.1016/j.memsci.2017.01.023.
[35] N. Li, et al., Static adsorption of protein-polysaccharide hybrids on hydrophilic modified membranes based on atomic layer deposition: anti-fouling performance and mechanism insight, J. Membr. Sci. 548 (73) (2018) 470–480, https://doi.org/10.1016/j.memsci.2017.11.063.
[36] G.R. Xu, et al., Layer-by-layer (LBL) assembly technology as promising strategy for tailoring pressure-driven desalination membranes, J. Membr. Sci. 493 (2015) 428–443, https://doi.org/10.1016/j.memsci.2015.06.038.
[37] R. Li, et al., Inkjet printing assisted fabrication of polyphenol-based coating membranes for oil/water separation, Chemosphere 250 (2020) 126236, https://doi.org/10.1016/j.chemosphere.2020.126236.
[38] M.R. Chowdhury, J. Steffes, B.D. Huey, J.R. Mccutcheon, 3D printed polyamide membranes for desalination, Science 361 (6403) (2018) 682–686.
[39] X.H. Ma, et al., Carbon nanotubes enhance permeability of ultrathin polyamide rejection layers, J. Membr. Sci. 570 (2019) 139–145, https://doi.org/10.1016/j.memsci.2018.10.055.
[40] C. Capparelli, C.R. Fernandez Pulido, R.A. Wiencek, M.A. Hickner, Resistance and permselectivity of 3D-printed micropatterned anion-exchange membranes, ACS Appl. Mater. Interfaces 11 (29) (2019) 26298–26306, https://doi.org/10.1021/acsami.8b04177.
[41] X.H. Ma, Z. Yang, Z.K. Yao, H. Guo, Z.L. Xu, C.Y. Tang, Interfacial polymerization with electrosprayed microdroplets: toward controllable and ultrathin polyamide membranes, Environ. Sci. Technol. Lett. 5 (2) (2018) 117–122, https://doi.org/10.1021/acs.estlett.7b00566.
[42] S. Yang, J. Wang, L. Fang, H. Lin, F. Liu, C.Y. Tang, Electrosprayed polyamide nanofiltration membrane with intercalated structure for controllable structure manipulation and enhanced separation performance, J. Membr. Sci. 602 (2020) 117971, https://doi.org/10.1016/j.memsci.2020.117971.
[43] M. Nasir, H. Matsumoto, M. Minagawa, A. Tanioka, T. Danno, H. Horibe, Preparation of PVDF/PMMA blend nanofibers by electrospray deposition: effects of blending ratio and humidity, Polym. J. 41 (5) (2009) 402–406, https://doi.org/10.1295/polymj.PJ2008171.
[44] K.W. Guarini, C.T. Black, S.H.I. Yeung, Optimization of diblock copolymer thin film self assembly, Adv. Mater. 14 (18) (2002) 1290–1294, https://doi.org/10.1002/1521-4095(20020916)14:18<1290::AID-ADMA1290>3.0.
[45] C.T. Black, R. Rulz, R.L. Sandstrom, Methods for forming improved self-assembled patterns of block copolymers, U. S. Jpn. Outlook 7 (953) (2008) 347.
[46] B. Akpinar, et al., Determining the effective density and stabilizer layer thickness of sterically stabilized nanoparticles, Macromolecules 49 (14) (2016) 5160–5171, https://doi.org/10.1021/acs.macromol.6b00987.
[47] S.T. Ahmed, D.E. Leckband, Protein adsorption on grafted zwitterionic polymers depends on chain density and molecular weight, Adv. Funct. Mater. 30 (30) (2020) 1–10, https://doi.org/10.1002/adfm.202000757.
[48] Y. Zhou, et al., Establishment of a physical model for solute diffusion in hydrogel: understanding the diffusion of proteins in poly(sulfobetaine methacrylate) hydrogel, J. Phys. Chem. B 121 (4) (2017) 800–814, https://doi.org/10.1021/acs.jpcb.6b10355.
[49] D. Whisnant, "Polymer Chemistry : polymer density, in: Polymer Chemistry, 2020.
[50] F. Yan, et al., Improving the water permeability and antifouling property of thin-film composite polyamide nanofiltration membrane by modifying the active layer with triethanolamine, J. Membr. Sci. 513 (2016) 108–116, https://doi.org/10.1016/j.memsci.2016.04.049.